ADVANCED FUNCTIONAL MATERIALS
www.afm-journal.de

High-Temperature Photochromism of Fe-Doped $SrTiO_3$ Caused by UV-Induced Bulk Stoichiometry Changes

Alexander Viernstein, Markus Kubicek, Maximilian Morgenbesser, Gregor Walch, Georg Christoph Brunauer, and Jürgen Fleig*

The impact of UV irradiation on Fe-doped $SrTiO_3$ (Fe:STO) single crystals is investigated at elevated temperatures. Illumination leads to incorporation of oxygen into the single crystals and thus to a decreasing oxygen vacancy concentration and oxidation of Fe^{3+} to Fe^{4+}. The Fe^{4+} ions cause a color change from transparent/brownish to black. This photochromic blackening due to stoichiometry changes at elevated temperatures is irreversible at room temperature, but annealing at high temperatures, for example at 700 °C, can restore the original stoichiometry and color. Absorbance changes due to UV irradiation are monitored by ex situ and in situ UV–vis spectroscopy experiments and changes in electrical properties are measured by van der Pauw measurements and in-plane electrochemical impedance spectroscopy. After 1140 min of illumination at 440 °C, for example, electrical measurements reveal a conductivity increase by more than a factor of 5 due to the enhanced hole concentration in blackened Fe:STO. In addition, UV illumination increases the oxygen chemical potential up to a calculated $p(O_2)$ of more than 10^9 Pa in Fe:STO. Hence, UV light can be used to tune the color, but also electrical properties of Fe:STO by directly impacting the bulk defect concentrations.

1. Introduction

$SrTiO_3$ (STO) with its cubic perovskite structure is one of the best investigated electroceramic materials.[1] It exhibits a bandgap energy of ≈3.2 eV[2] at room temperature and may serve as a model perovskite,[3] as high-k dielectric for grain boundary barrier layer capacitors,[4,5] in sensor applications,[6,7] and as substrate for superconductors.[8] Moreover, it is a promising material in the field of resistive switching,[9] a mixed conductor for fuel cell electrodes,[10] and can be used as anode in Li-ion batteries.[11]

In order to understand the properties of mixed conductors, knowledge of their defect chemistry is essential. Therefore, many studies dealt with the influence of $p(O_2)$, temperature and doping on the properties of $SrTiO_3$. Its conductivity changes as a function of these three parameters, varying from mainly electronic (electrons or electron holes as charge carriers) to ionic (via oxygen vacancies).[12–16] For example, for a doping level of 1 mol% Fe and 850 °C the ionic regime reaches from a $p(O_2)$ of 10^{-7} to 10^{-2} Pa. Below this partial pressure region, electronic n-type conductivity is dominant and above the material is p-type conductive.[12] Fe as p-type dopant in $SrTiO_3$ (Fe:STO) also introduces energy levels within the bandgap[17] as well as $Fe–V_O$ associates. This causes absorbance and color changes in Fe:STO.[18] Strong absorption bands at about 440 and 590 nm are usually attributed to Fe^{4+} ions resulting by trapping of holes in the oxidizing $p(O_2)$ range.[19–22] However, the exact oxidation state of Fe is challenging to determine due to the partly covalent bonds with oxygen and the low Fe concentrations in specimen in this study. X-ray photoelectron spectroscopy on similar perovskites with larger Fe content showed values between 3+ and 4+.[23,24] For simplicity, we adopt the common "Fe^{4+}" nomenclature as synonym for a trapped electron hole in Fe:STO. Measuring the absorbance of Fe:STO can thus be used to quantify Fe^{4+} concentrations and via defect chemical calculations also the oxygen vacancy concentrations in Fe:STO. Time dependent absorbance changes after $p(O_2)$ jumps are often used to determine kinetic parameters of Fe:STO (oxygen diffusion and oxygen exchange coefficients).[1,25,26]

However, in STO the individual defect concentrations can not only be changed by varying $p(O_2)$ or temperature, it is also possible to modify defect concentrations by applying a voltage.[16,19,27–29] Moreover, voltage-induced processes are employed to obtain resistive switching in oxides for memristive applications.[9,30–32] Frequently, such voltage driven stoichiometry changes in Fe:STO also lead to local color changes and the corresponding phenomenon is then called "electrocoloration."[27,33] Similar phenomena have been observed in many other oxides, e.g., in yttria-stabilized zirconia (they are often called "electrochemical blackening").[34,35]

A. Viernstein, Dr. M. Kubicek, M. Morgenbesser, Dr. G. Walch, Dr. G. C. Brunauer, Prof. J. Fleig
Institute of Chemical Technologies and Analytics
TU Wien
Getreidemarkt 9 164/EC, 1060 Vienna, Austria
E-mail: markus.kubicek@tuwien.ac.at

The ORCID identification number(s) for the author(s) of this article can be found under https://doi.org/10.1002/adfm.201900196.

DOI: 10.1002/adfm.201900196

Recently, it was shown that UV illumination at elevated temperatures can also change the oxygen bulk stoichiometry and thus all defect concentrations in oxides. For example, in STO single crystals the bulk oxygen vacancy concentration could be reduced by UV exposure, i.e., the oxygen chemical potential was increased after illumination. This lead to a battery-type voltage in an electrochemical cell with a STO electrode operating at 360 °C.[36] Also the related kinetic effect of UV light, namely the enhancement of the oxygen incorporation rate, was described for Fe:STO.[20] Moreover, it was reported that defect concentrations in STO substrates are affected by the UV light of the plasma plume during pulsed laser deposition.[37]

In analogy to the voltage-induced electrochromism due to a redistribution of oxygen vacancies in Fe:STO (electrocoloration), one might thus also expect existence of light-induced photochromism. Photochromic effects based on color centers have been frequently reported for oxides with metals ($SrTiO_3$, TiO_2, and many other oxides).[21,38–47] However, those photochromic experiments usually take place around room temperature or much below and the corresponding phenomena are not caused by oxygen stoichiometry changes of the bulk under illumination. Rather, they mostly involve changed occupancies of defect states (activation or deactivation of color centers by light). Some other processes are also discussed such as oxidation and reduction of Ag in silver modified titania.[40] However, all those photochromic effects are not truly analog to the electrocoloration process of oxides mentioned above, since they do not change the oxygen vacancy concentration. To the best of our knowledge this was not investigated so far.

In this study, changes in color and conductivity after UV irradiation of Fe-doped STO are investigated by means of UV–vis absorption spectroscopy, van der Pauw measurements and in-plane electrochemical impedance spectroscopy (EIS). The predominant electronic charge carrier in our measurement conditions were holes. Strong photochromic effects were found, with a UV-induced color change from transparent/brownish to black. The results are discussed in terms of the standard defect model of Fe:STO,[14] i.e., based on the defect chemical reactions for trapping/detrapping of holes (1), oxygen incorporation, and release (2) and electron–hole generation/recombination (3)

$$Fe_{Ti}^{x} \rightleftharpoons Fe'_{Ti} + h^{\bullet} \quad (1)$$

$$\frac{1}{2}O_2 + V_O^{\bullet\bullet} \rightleftharpoons O_O^{x} + 2h^{\bullet} \quad (2)$$

$$\text{nil} \rightleftharpoons e' + h^{\bullet} \quad (3)$$

Here, $h^{\bullet}$ denotes mobile electron holes while Fe_{Ti}^{x} indicates the nominal Fe^{4+} state with a trapped hole, irrespective of the exact atomistic localization of this trapped hole (see above). All our experiments can be explained by an oxygen uptake of Fe:STO upon UV irradiation and thus oxidation of Fe from Fe^{3+} to Fe^{4+} in the bulk of the oxide. From the thermodynamic data of the defect chemical reactions we can estimate the chemical potential change in the bulk of Fe:STO induced by UV light.[14] This photochromic effect is not only attractive from a basic science point of view and for self-regulating optical transmittance of oxides, its fundamental mechanistic aspects may also be of high interest regarding applications in the field of light driven CO_2 or H_2O splitting or photocharging of batteries.[48]

2. Results and Discussion of Optical Absorbance Measurements

2.1. Ex Situ Absorbance Measurements

Figure 1 displays a sketch of the photochromic effects and the (defect) chemical processes in Fe:STO single crystals investigated in this study. UV irradiation at 350–440 °C causes oxygen incorporation by filling oxygen vacancies and is associated with a change of the color; annealing at 700 °C recovers the color and defect state. For the optical characterization of the photochromic effects, two approaches (ex situ and in situ measurements) were employed. In the first approach (ex situ), specimens were blackened by UV exposure at 440 °C in a tube furnace and the absorbance was measured subsequently at 200 °C surface temperature in an UV–vis setup with heating stage. Four absorption spectra are shown in **Figure 2**. First, the pristine Fe:STO single crystal with a brownish tint was measured after exposure to 700 °C for 180 min in air and quenching to room temperature in less than 5 min to preserve the vacancy concentration established at 700 °C. Second, the sample was investigated after UV illumination at 440 °C for 210 min. The third spectrum was taken after another 930 min under UV light at 440 °C on the now black single crystal. At room temperature this blackened state is frozen-in and does not change.

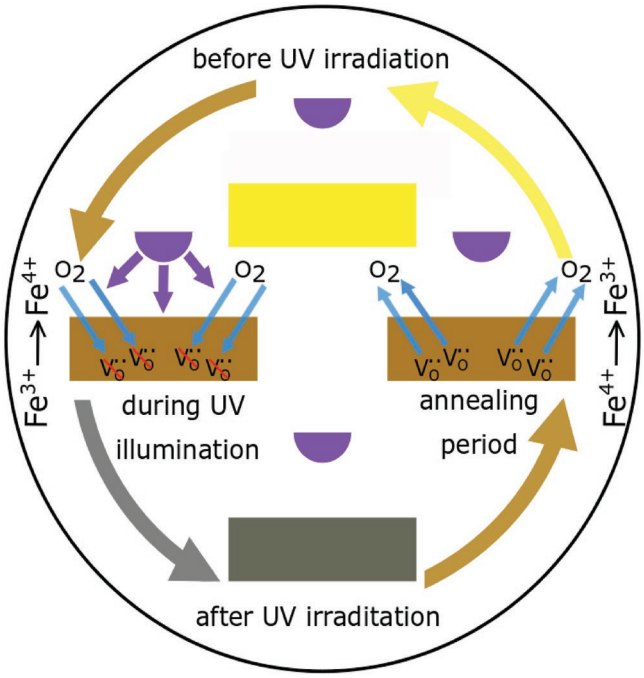

Figure 1. Basic concept of the UV coloration experiment: during UV illumination oxygen is incorporated into Fe:STO, simultaneously Fe^{3+} is oxidized and the color of the single crystal changes from transparent/brownish to dark brown/black. After annealing at 700 °C for 720 min in air, the original composition/color is restored.

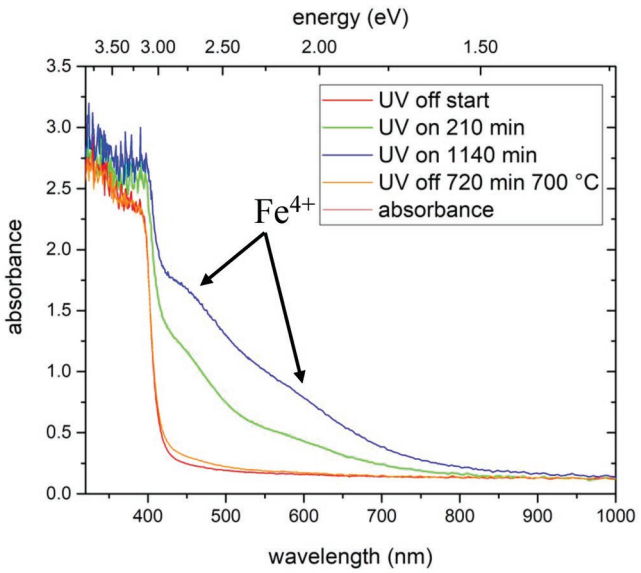

Figure 2. UV–vis spectra of the ex situ measurements, all obtained at 200 °C surface temperature—starting with a single crystal after 700 °C (180 min) annealing (red line). Due to UV illumination at 440 °C in air, the absorbance increases to the green line (UV on for 210 min) and finally to the blue line (UV on for 1140 min): two broad Fe^{4+} absorption bands appear at about 450 and 600 nm. After 720 min at 700 °C without irradiation, the absorbance nearly reaches the initial state (orange line).

However, the initial state can be re-established by annealing at 700 °C in air (>720 min), see fourth spectrum. Photographs of a Fe:STO sample in **Figure 3**a show the drastic photochromic effect. Moreover, the diffusive nature of this effect is revealed by irradiating only a part of a Fe:STO crystal at 440 °C (Figure 3b). Also, the parts of the sample covered during UV exposure change their color with a clear in-plane coloration profile. In an optical microscope the diffusion front appears homogeneous to the micrometer level, we consequently ascribe the curvature of the blackened zone in Figure 3b to the shape of the waveguide. Hence, existence of the strong in-plane profile indicates that a bulk diffusion process plays an important role in the coloration. As detailed in the following, it comes from the incorporation of oxygen, which diffuses through the specimen, fills the oxygen vacancies, and changes the properties of the whole Fe:STO single crystal. Effects of dislocations which are sometimes discussed as possible line-shaped fast diffusion paths[49] or oxygen-reduced zones[50,51] were not observed.

After UV irradiation, not only the average absorbance is increased over the whole spectral width, but particularly two broad absorption bands appear around 450 and 600 nm in the UV–vis absorption spectra measured at 200 °C. The already strong absorbance after 210 min upon UV is further increased by longer exposure. This becomes even better visible when subtracting the absorbance of an undoped $SrTiO_3$ single crystal (Crystec, Germany) (**Figure 4**a). The two broad absorption bands in Fe:STO are commonly attributed to Fe^{4+}, while Fe^{3+} exhibits almost no absorption in the visible regime.[15,19,20,52,53] The enhanced absorbance and the two Fe^{4+} bands disappear after the annealing step at 700 °C. This strongly suggests an oxidation of our Fe:STO samples upon UV, i.e., an oxygen uptake with a Fe^{3+} to Fe^{4+} transition and a decrease of the oxygen vacancy concentration,[19,20] in accordance with the defect chemical model of Fe:STO.[14]

Hence, we have experimental evidence that the defect chemical state of the entire Fe:STO crystal can be changed by UV exposure. This is very different from reported photochromic effects in transition metal oxides occurring at room temperature or below, see Introduction. In those experiments, UV light modifies electron occupation of defect related color centers, and elevated temperatures quickly annihilate the photochromism. In our experiments absorbance effects due to compositional changes (oxygen vacancy annihilation) at elevated temperatures.

A closer look at Figure 4 reveals that the single crystals probably contain a small amount of Fe^{4+} already before UV irradiation at ambient $p(O_2)$. This is visible as brownish tint and leads to a small peak in the UV–vis spectra at 405 nm (measured at 200 °C) or 430 nm (measured at 440 °C), though no absorption band can be found in the region of 590/600 nm. During UV illumination, the Fe^{4+}-related peak becomes much stronger and its maximum or plateau shifts to slightly higher wavelengths (420–430 nm at 200 °C and 440 nm at 440 °C). Additionally, a second absorption band appears at around 600 nm. In literature, an additional charge transfer from Fe^{4+} to Fe^{5+} was reported for photochromic absorption experiments far below room temperature, with bands at 623 and 490 nm.[22] However, those bands were never observed here.

2.2. In Situ Absorbance Measurements

In a second approach, in situ blackening was performed, i.e., quasisimultaneous UV illumination and UV–vis absorption measurement. More specific, a 360 min UV exposure at 440 °C was interrupted regularly for less than a minute to obtain absorption spectra. After this UV exposure the Fe:STO single crystal was equilibrated for more than 5200 min at 440 °C, accompanied by further spectroscopic measurements. As in the ex situ experiment, an increase of the absorbance was observed under UV light (**Figure 5**a). The two Fe^{4+} bands, however, can no longer be distinguished at the temperature of 440 °C, even after subtracting the absorbance of a nominally undoped STO single crystal (Figure 4b). The increased absorbance vanished slowly, and almost completely, during the subsequent long re-equilibration at 440 °C (Figure 5b).

According to our interpretation, and in accordance with all our data, the Fe^{4+} concentration increase under UV light is caused by an oxygen uptake and the corresponding decrease of the oxygen vacancy concentration in the entire bulk of Fe:STO. After turning the UV light off and remaining at the elevated temperature, oxygen is slowly released from the crystal, and the original optical absorption spectrum is nearly received after some time. However, this reduction step is much slower than the oxidation under UV light. In the in situ experiment, blackening was obtained after 360 min at 440 °C, while it took more than 4200 min at 440 °C to regain the spectrum of the pristine specimen. This is in line with earlier measurements by Merkle et al., who found that oxygen incorporation into Fe:STO is accelerated under UV.[20]

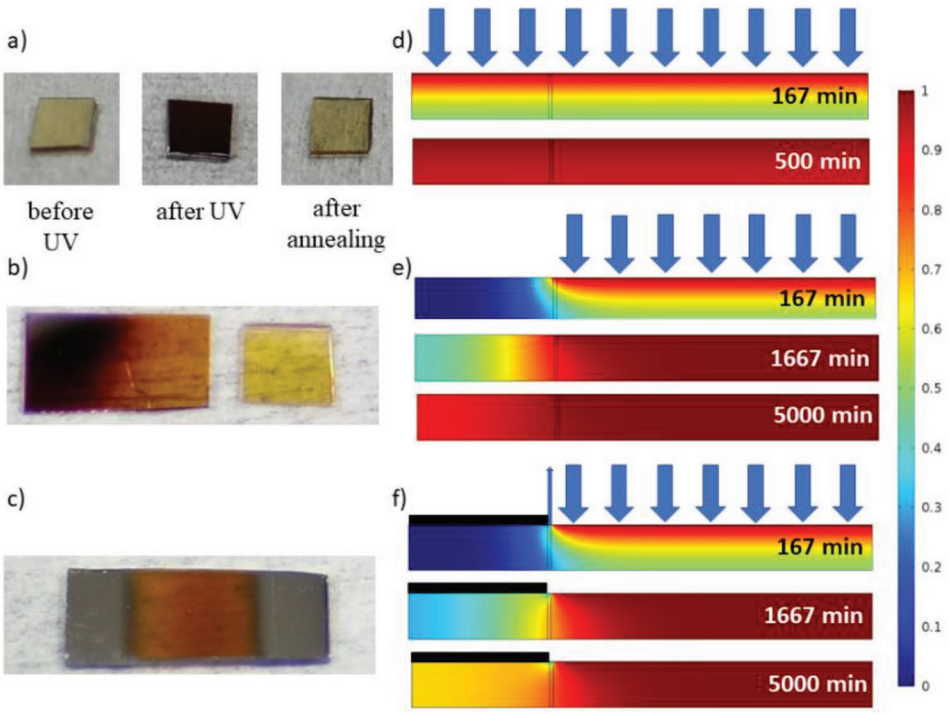

Figure 3. a) Photograph of a pristine Fe:STO with a transparent/brownish tint, blackened specimen after 1140 min under UV light at 440 °C and after annealing the blackened sample for 720 min at 700 °C—again transparent/brownish tint. b) After equilibration in air at 700 °C right half of the sample was illuminated for 1380 min at 440 °C. Brown color of the unexposed part and the in-plane color gradient indicates oxygen diffusion. For comparison also a sample without UV exposure is shown on the right. c) Fe:STO sample with two Pt electrodes (used for impedance studies) after UV illumination. A slight in-plane gradient suggests that incorporation takes place exclusively between the electrodes and possibly oxygen is again released at the three-phase boundary. d) Two calculated oxygen diffusion profiles in a 0.5 mm thick sample; oxygen incorporation along the entire (illuminated) surface is assumed. The profiles are based on a diffusion coefficient of $D_O^\delta = 1 \times 10^{-7}$ cm^2 s^{-1} and a surface exchange coefficient of $k_O^\delta = 1 \times 10^{-4}$ cm s^{-1}; top profile after 167 min, lower after 500 min. e) Three calculated diffusion profiles, corresponding to sample b). Oxygen incorporation takes place only on the right side, indicated by the blue arrows (parameters as in (d))). The slow in-plane diffusion is obvious. f) Diffusion profile calculated for the situation shown in (c) after 167, 1667, and 5000 min with oxygen release at the three-phase boundary ($k_O^\delta = 1 \times 10^{-4}$ cm s^{-1} with outer concentration at the initial state (i.e., at 0).

For oxygen equilibration of similar Fe:STO samples after $p(O_2)$ changes, surface exchange limitation is suggested below 400 °C and diffusion limitation above 500 °C.[23] However, as the oxygen uptake rate is strongly accelerated by UV, we assume that oxygen diffusion in the single crystal rather than oxygen incorporation determines the time dependence of establishing a new oxygen vacancy concentration and thus also of the new Fe^{4+} concentrations (c) in our Fe:STO. Accordingly, the following Equations (4) and (5) for long time diffusion in a finite sample are applied to describe our obtained normalized absorbance A'[54]

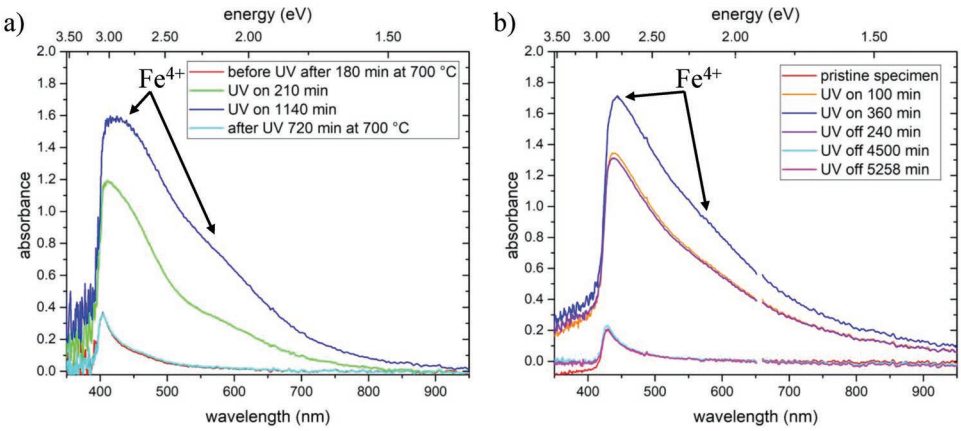

Figure 4. Absorption spectra of Fe:STO minus the absorption spectra of undoped STO measured a) ex situ at 200 °C and b) in situ at 440 °C. Several states are compared (UV blackening as well as postannealing ("UV off") was done at 440 °C in both cases).

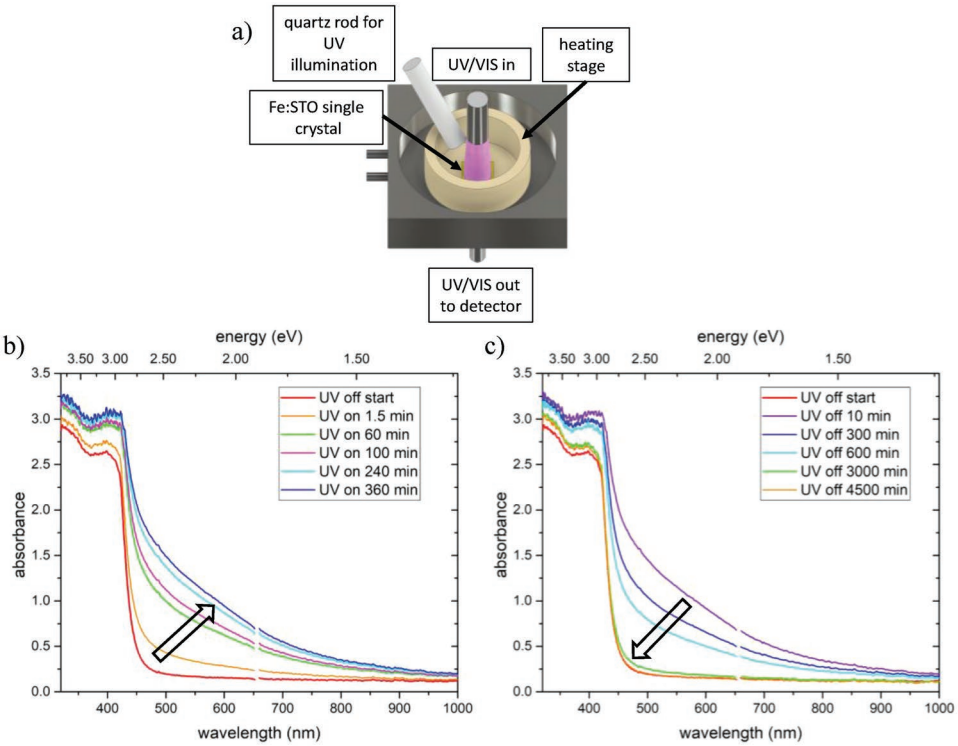

Figure 5. a) In situ blackening/coloration was performed in the UV–vis setup. b) Absorption spectra at 440 °C before (red line) and during UV illumination (up to 360 min, violet line). The absorbance is increased over the whole spectral width. c) Absorbance of the pristine single crystal (red line) and bleaching of the blackened crystal at 440 °C, after the UV–LED was turned off. After 4500 min, the initial absorbance was nearly re-established (orange line)—further heating did not change the absorbance.

$$A' = \frac{A(t) - A(0)}{A(\infty) - A(0)} = \frac{c(t) - c(0)}{c(\infty) - c(0)} = 1 - B * \exp\left(-\frac{1}{\tau^{\delta}} * t\right) \quad (4)$$

$$\tau^{\delta} = \frac{4L^2}{\pi^2 * D_O^{\delta}} \quad (5)$$

Herein, B represents a prefactor, which ideally becomes $\frac{8}{\pi^2}$ for long time fits, τ^{δ} is the time constant, determined by the sample thickness (L = 0.05 cm) and the oxygen diffusion coefficient D_O^{δ}.

The normalized absorbance changes according to Equation (4) and the corresponding fits can be seen in **Figure 6** for the energies related to the Fe^{4+} bands and for the point of inflexion of the entire absorption spectra. Reasonable fits are possible between 15 and 360 min, though the B factor is between 0.51 and 0.65 instead of the ideal 0.81. This might be partly due to the fact that Equation (4) only describes the time dependence for small changes and here we face quite large changes.[54] Still we think that an estimation of D_O^{δ} can be obtained from these fits. Oxygen diffusion coefficients of 1.4×10^{-7} cm^2 s^{-1} for the normalized absorbance change at 590 nm and 1.6×10^{-7} cm^2 s^{-1} at 440 nm result at 440 °C. This is in the range of oxygen chemical diffusion coefficients reported for similar doped Fe-doped STO at 440 °C in 10^4 Pa $p(O_2)$ (about 10^{-7} cm^2 s^{-1}).[26,55] Accordingly, our analysis further supports the interpretation of UV-induced oxygen incorporation and bulk diffusion as the origin of the observed photochromism. In Figure 3b, a finite element calculation shows the oxygen diffusion profile for $D_O^{\delta} = 10^{-7}$ cm^2 s^{-1} and fast oxygen exchange after 167 min, i.e., with about 50 % of the final concentration change already at the bottom side of the 0.5 mm thick crystal.

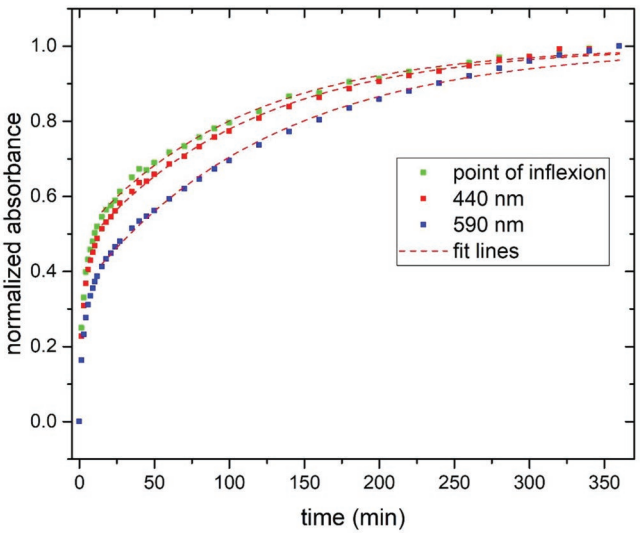

Figure 6. Evolution of the normalized absorbance A' with time under UV illumination at 440 °C; all three wavelengths (440, 590, and the point of inflexion at 432 nm) show a similar behavior. The long-time fits are marked with red dashed lines.

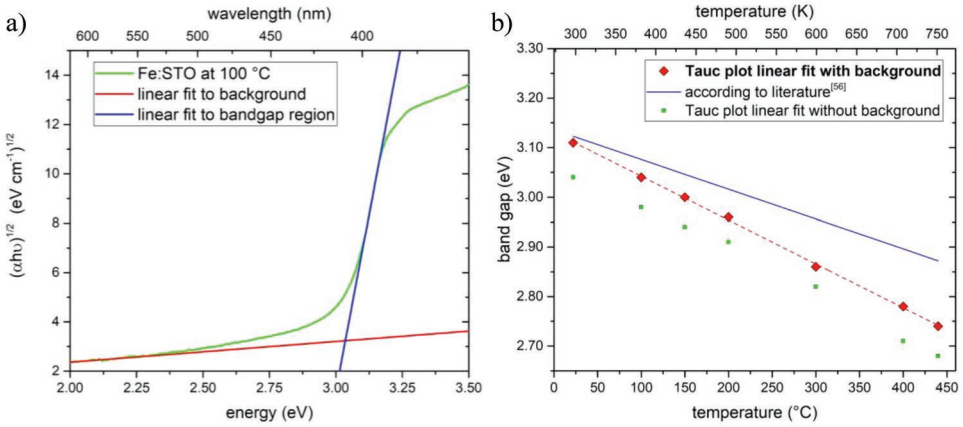

Figure 7. a) Tauc plot of pristine Fe:STO at 100 °C measurement temperature, with linear fits to the bandgap region (blue line) and to the background (red line). b) Bandgap evolution with temperature: the green squares refer to the intersection of a linear fit to Tauc plots in the bandgap region and the $h\upsilon$-axis and red diamonds represent the bandgap energy resulting from the intersection between a linear fit to the bandgap region and to the background.

2.3. Analysis of the Bandgap Energy

The photon energy ($h\upsilon$) of the UV–LED used here (3.4 eV/365 nm) is larger than the indirect Fe:STO bandgap (in the range of 3.1 eV at room temperature and below 3.0 eV at elevated temperatures, see **Figure 7**b). Electron excitation is thus possible from the valence band, mainly consisting of O 2p states, to the conduction band Ti 3d states.[15,56] Indirect bandgap energies can be estimated from Tauc plots of $(\alpha h\upsilon)^{1/2}$ against $h\upsilon$; α = absorbance/L.[57] Two approaches can be found in literature: either the indirect bandgap energy is referred to the intersection between a linear fit to the Tauc plot data in the bandgap region and the $h\upsilon$-axis[57,58] or the bandgap is deduced from the intersection between two linear fits, one to the data in the bandgap region and one to the background data.[59] Both approaches are exemplified in Figure 7a for the absorption spectrum of a pristine sample at 100 °C measurement temperature. In Figure 7b, the temperature dependent bandgap obtained by the two methods is shown for a pristine Fe:STO single crystal. Bieger et al.[55] described the bandgap variation with temperature in 0.03-0.29 mol% Fe-doped STO by Equation (6)

$$E_g = E_g^0 - \beta * T \tag{6}$$

Herein E_g^0 (3.3 eV) is the bandgap at 0 K. The temperature coefficient β was determined to be 6×10^{-4} eV K^{-1}, the corresponding values are also shown in Figure 7b.[55] We receive an E_g^0 of 3.31 eV (green data points in Figure 7b) or 3.37 eV (if the background is considered) and β of $8.7 \pm 0.29 \times 10^{-4}$ eV K^{-1} or $8.8 \pm 0.11 \times 10^{-4}$ eV K^{-1}, respectively. We consider the background corrected bandgap energies as more reliable, see also below (i.e., $E_g = 3.37$ eV $- 8.8 \times 10^{-4}$ eV K^{-1}* T).

The same type of analysis can be applied to the spectra measured upon or after UV illumination and thus with strong Fe^{4+} bands. During UV irradiation at 440 °C, $(\alpha h\upsilon)^{1/2}$ as a function of $h\upsilon$ starts to tilt. As a consequence, the slopes of the linear fits to the bandgap region decrease, resulting in intersections with the $h\upsilon$-axis at lower energies (**Figure 8**). Hence, if only these fits are considered for bandgap evaluation, the bandgap seems to decline under UV irradiation (**Figure 9**). Keeping the temperature constant and turning the UV light off, then seems to indicate an increase of the bandgap energy to the initial energy. However, if the intersection with a linear fit to the background is used (cf. red and blue lines in Figure 8) the bandgap does not change at all, neither under UV nor after UV. The evaluation leading to unchanged bandgaps of 2.74 eV at 440 °C is considered superior. The reason is the rather small actual compositional change from filling of about 10^{18} cm^{-3} oxygen vacancies (counterbalancing the Fe^{3+} dopants), compared to the $\approx 5 \times 10^{22}$ cm^{-3} oxygen atoms in STO. Therefore, we expect the relative energy of valence versus conduction band—the bandgap—to remain the same, even though the Fermi level or trapping states may vary strongly even due to such small compositional changes.

3. Results and Discussion of Electrical Measurements

3.1. Van der Pauw Measurements—DC Conductivity

According to our interpretation of the optical experiments, oxygen is incorporated under UV light. Hence, the ionic and electronic conductivity of Fe:STO should also strongly change. Conductivity changes were monitored either after UV exposure by DC conductivity van der Pauw[60,61] measurements or during illumination by in-plane electrochemical impedance spectroscopy. For van der Pauw measurements, pristine and blackened samples were investigated. Blackening was done under UV for 1140 min at 440 °C in ambient air. After UV irradiation four Pt electrodes were sputtered onto the corners of the crystals.

In **Figure 10**, an Arrhenius-type plot of the conductivity can be seen for pristine and blackened samples. Blackened Fe:STO exhibits a much higher DC conductivity than pristine Fe:STO. This clearly indicates defect chemical changes upon UV irradiation. The first heating of the blackened Fe:STO lead to a slight decrease of the conductivity, probably due to some oxygen release. A second temperature cycle did not further modify the

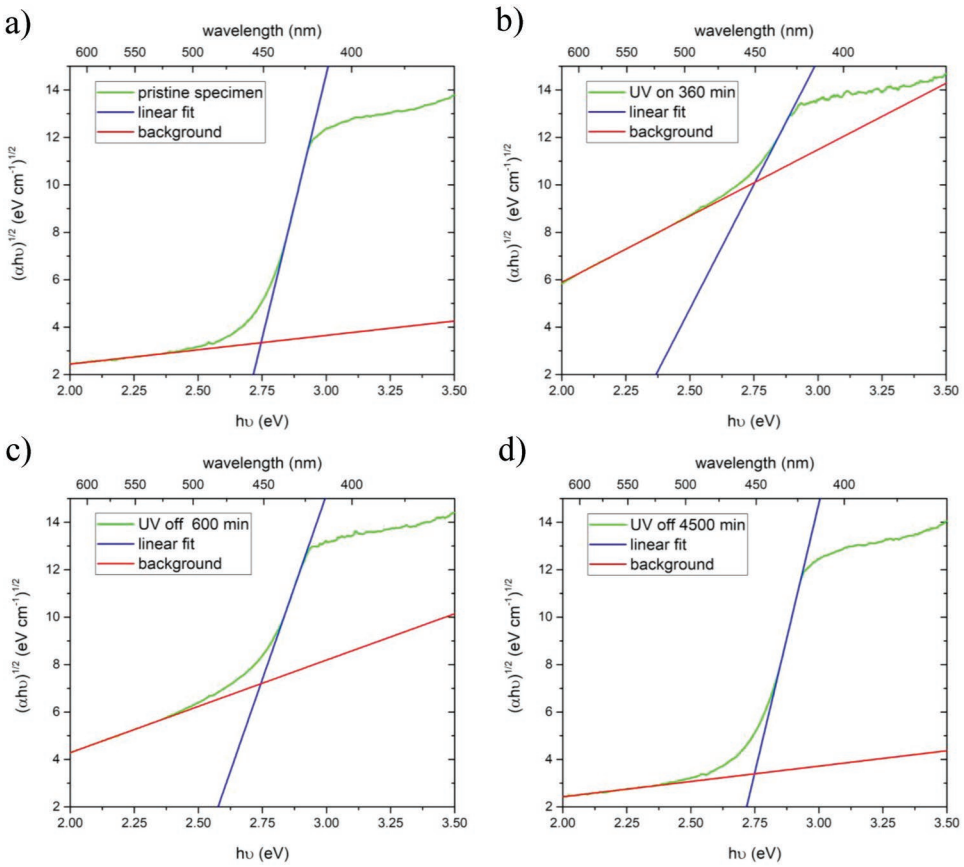

Figure 8. Tauc plots with linear fits to the bandgap region (blue lines) and to the background (red lines) at 440 °C during in situ blackening and bleaching. Spectra of the pristine Fe:STO crystal a), after 360 min of UV light illumination b), after the UV light was turned off for 600 min c) and 4500 min d).

sample. Pristine Fe:STO exhibits an activation energy of 0.95 eV and the blackened specimen possesses activation energies of 0.87 eV during the first heating period and 1.10 eV for further temperature cycles. According to the chemical defect model of Fe:STO,[14] the hole conductivity of equilibrated Fe:STO should be 1.5×10^{-5} S cm^{-1} at 350 °C in air and this is very close to the values measured for the pristine sample. The activation energy of pristine and blackened Fe:STO largely reflects the

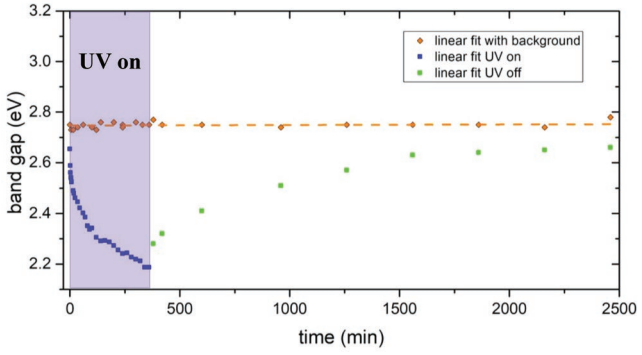

Figure 9. Bandgap evolution with UV exposure at 440 °C. E_g is determined from intersections between a linear fit to the bandgap region and the $h\upsilon$-axis or a linear fit to the background.

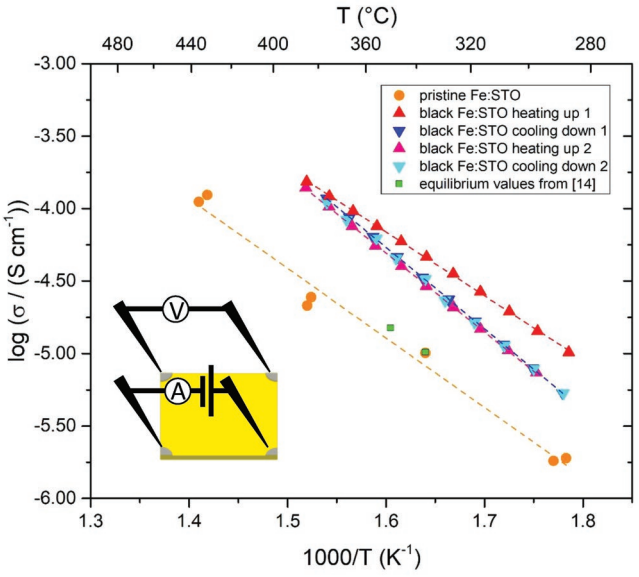

Figure 10. Arrhenius plot obtained by DC conductivity van der Pauw measurements (setup is sketched in the inset); the blackened specimen (triangles) exhibits an enhanced conductivity compared to pristine Fe:STO (orange dots) and the calculated values (green squares), obtained from equilibrium thermodynamic data.[14]

temperature dependent hole concertation due to hole-trapping (Fe^{4+} formation) with an activation energy of 0.75–0.95 eV[14,55] in the investigated temperature range. A much smaller part comes from an increase of mobility of mobile holes with temperature, and therefore a total activation of ≈1 eV is in accordance with literature. From the increased conductivity of the blackened specimen we can thus conclude an increased hole conductivity. This enhanced mobile hole concentration also implies an increased trapped hole (i.e. Fe^{4+}) concentration in accordance with Equation (1) and all optical measurements. Moreover, it implies a reduced oxygen vacancy concentration and thus again supports our interpretation of, oxygen incorporation upon UV.

3.2. In-Plane AC Conductivity Changes

Impedance spectra were recorded between two Pt-stripe electrodes on Fe:STO under UV illumination at 350 and 400 °C. At higher temperatures, the high-frequency semicircle shifts toward even higher frequencies so that its capacitance could not be evaluated. Spectra before and during UV exposure are shown in **Figure 11**. The largest arc of the spectra at high frequencies can be attributed to the bulk resistance of Fe:STO (in parallel to the geometric capacitance of the Fe:STO sample). The low frequency features are most probably caused by metal electrode related processes such as space charges. These features of the electric measurements are not further considered, as the bulk changes are predominant and sufficient to explain all optical and electric effects. Hence, a fit of the main high-frequency arc using an RC element gives the total bulk resistance and this can be used to calculate the bulk conductivity. For the sake of simplicity, we neglect the two dimensionality of the current flow between the two stripe electrodes and calculate the conductivity simply from the stripe distance and the sample thickness. The time dependence of this conductivity is analyzed in the following.

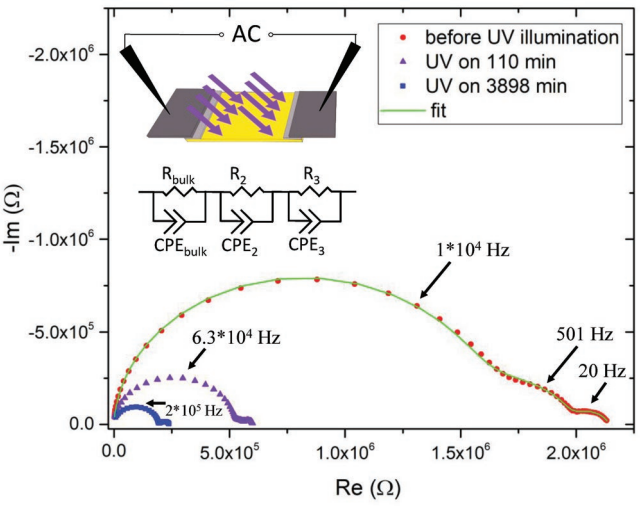

Figure 11. Impedance spectra before and during UV irradiation at 350 °C measured in the sketched manner, with a corresponding fit to the given equivalent circuit consisting of three R-CPE elements (CPE: constant phase element). The high-frequency arc with the largest individual resistance can be attributed to the bulk conductivity and permittivity of Fe:STO. For higher temperatures under illumination, the first semicircle shifts to very high frequencies >10^6 Hz which are no longer accessible, and the resulting axis offset has to be used for determination of the resistivity.

The calculated in-plane conductivity of the pristine sample is about 7.4×10^{-6} S cm^{-1} at 350 °C. Upon UV light, the conductivity increases quickly by nearly a factor of 4, followed by a further but much slower conductivity increase, reaching 6.2×10^{-5} S cm^{-1} after more than 4000 min. An end of this slow conductivity variation could not be observed over the experimental duration. By turning off the UV illumination, a quick and small conductivity drop was obtained, followed by a slow decline in conductivity. It seems to level out at 1.9×10^{-5} S cm^{-1} but the initial value is not reached at 350 °C. A second UV irradiation cycle leads to an even higher conductivity with a maximum at 8.4×10^{-5} S cm^{-1} before turning the light off, followed by a conductivity relaxation in dark. The measurement series in Figure 10a was followed by an equilibration step at 700 °C for 720 min to re-equilibrate the specimen. In a second experiment at 400 °C, the conductivity evolution shows the same trends as before. An initial conductivity of 5.6×10^{-5} S cm^{-1} and a maximum at 2.8×10^{-4} S cm^{-1} (upon UV) and 2.6×10^{-4} S cm^{-1} (after UV) were found.

The "step-like" initial conductivity changes in **Figure 12** may include some photoconductivity due to the excitation of electrons from the valence to the conduction band by UV light. Moreover, some heating of the specimen by the UV irradiation contributes to the first conductivity increase. We can estimate the upper limit of the temperature effect from the first data point which is obtained from the initial impedance spectrum completed 6.5 min after switching the light on or off. From our Arrhenius-type conductivity measurements in Figure 10, we can relate the observed conductivity jump upon switching either on or off time to a temperature jump. We consider the jump for turning the light off more reliable for estimating the temperature change than the jump for switching on, as the conductivity change due to stoichiometry variation also contributes to the first data point. This change is significantly slower off than on and thus less overestimation of the temperature effect is expected when analyzing the off jump. Both off jumps in the measurement shown in Figure 12 are a factor 1.08 in conductivity or ≈3 °C (calculating with $E_a = 0.95$ eV and $T = 400$ °C). Hence, we can estimate 3 °C as the upper limit of UV-induced temperature changes in this experiment.

The changes following this quick jump are the true electrical counterpart to the absorbance changes upon UV irradiation. Those establish slowly under UV and relax even slower after UV exposure, i.e., on the time scale of many hours. These changes are again attributed to incorporation/release of oxygen into/out of Fe:STO under/after UV and thus to changes in defect concentrations and hole conductivity. One might expect that changes of the absorbance at 440 °C in Figure 5 and of conductivity at 400 °C in Figure 12b should take place on similar time scales. However, this is not the case; a steady state has not been reached in the impedance experiment. This continuing conductivity change on a long time scale is most probably simply a consequence of the stripe electrode geometry: in order to reach the stripe electrodes the current has to flow also in Fe:STO beneath the stripes and thus in regions without UV

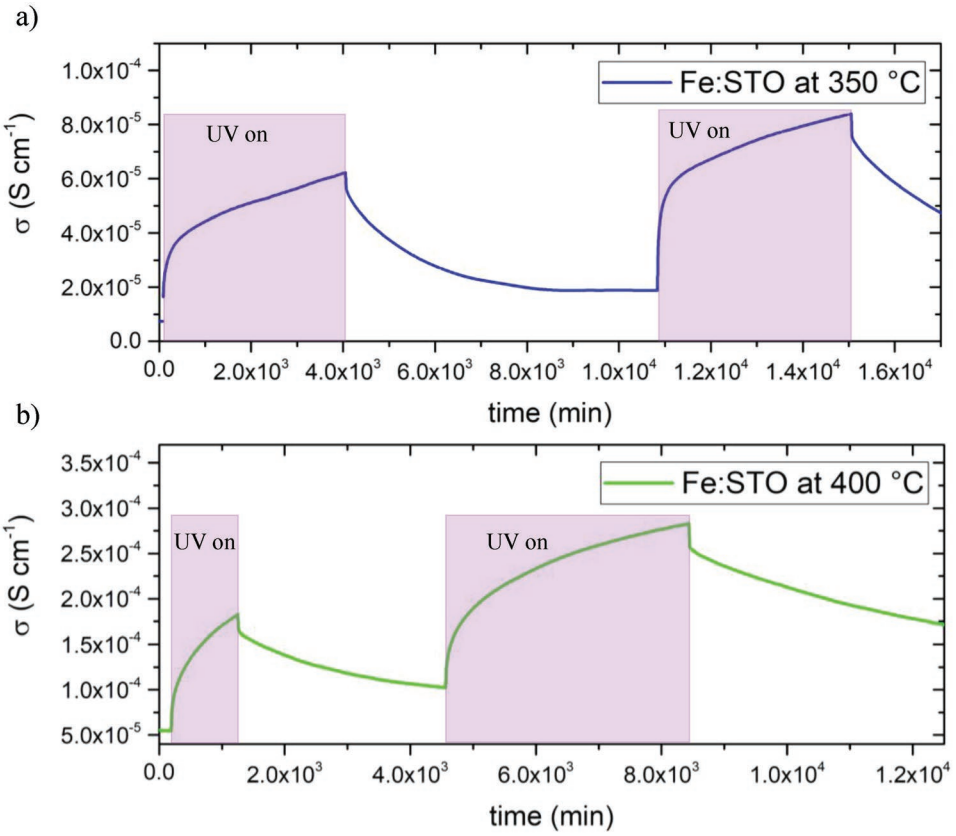

Figure 12. In-plane conductivity at a) 350 °C and b) 400 °C under UV on/off. Between these two experiments, the sample was annealed at 700 °C for 12 h to bleach the blackened sample.

illumination. Those bulk regions can also change their defect chemistry under UV due to in-plane diffusion of oxygen. However, this change takes place on a much longer time scale. This is illustrated by finite element calculations (Figure 3e). While after 167 min the illuminated regions are already strongly filled with oxygen, the diffusion front has only slightly penetrated the region beneath the electrodes (only half a sample is shown in Figure 3d). This sample part thus still exhibits a low conductivity and contributes a substantial serial resistance. Even after 5000 min oxygen stoichiometry and thus conductivity changes are ongoing beneath the electrodes. This prolongs the conductivity changes upon UV drastically.

These effects are even aggravated by the tendency of Pt/Fe:STO three phase boundaries to equilibrate with the gas phase, i.e., to annihilate the UV effect. An exemplary calculated oxygen profiles can be found in Figure 3f. The concentration front reaches the region beneath the stripes even slower and this further increases the time constant. The importance of Pt/Fe:STO interfaces was also observed in a UV experiment with a porous Pt layer on the bottom side of a Fe:STO single crystal. In this case, strong blackening was not possible due to oxygen being pumped into Fe:STO on top but leaving the crystal again at the catalytically active, non-illuminated bottom side. Accordingly, conductivity experiments with Pt electrodes on the non-illuminated bottom side qualitatively showed very similar results as in Figure 12 with long equilibration times for the conductivity increase alongside blackening and the decrease alongside bleaching.

Summarizing, the two retarding processes (in-plane diffusion and TPBs) strongly increase the time constant of the conductivity changes during UV illumination compared to the absorbance experiment. Owing to the same reasons also the re-equilibration after UV has to be much slower. This is further aggravated by the slower rate of oxygen release in dark compared to the oxygen incorporation upon UV. Therefore, a significant stoichiometry change is still present before the second UV illumination sets in in Figure 12. Only high-temperature annealing would have brought the sample back to the original state. Accordingly, the initial conductivity value of the second UV exposure is higher than for the first UV exposure. The still existing "stoichiometry offset" from the first UV illumination also causes the higher final conductivities in Figure 12 reached during the second UV illumination.

3.3. Estimating the Chemical Potential Change Caused by UV Light

Finally, we may use the defect chemical model of Fe:STO[14] to get a quantitative idea of the oxygen chemical potential changes ($\Delta\mu_{O_2}$) resulting from UV light. This quantitative estimate is gained from the data of the conductivity measurements. First, we calculate the $p(O_2)$, which is theoretically needed to obtain the measured in-plane conductivities of the blackened samples immediately after the conductivity drop when turning

UV off (7.9×10^{-5} S cm^{-1} at 350 °C and 2.6×10^{-4} S cm^{-1} at 400 °C). From the thermodynamic data of all defect equilibria and the charge carrier mobilities of Ref. [14], we find that the UV-induced oxygen incorporation caused the oxygen potential (after UV illumination) to increase to a $p(O_2)$ of 4.3×10^8 Pa respectively 8.4×10^8 Pa, corresponding to a $\Delta\mu_{O_2}$ of 536 meV at 350 °C and 618 meV at 400 °C, both compared to 2×10^4 Pa. These values are only lower estimates of the changes since obviously the steady state conductivity has not been reached in the experiments. Extrapolation of the ex situ van der Pauw conductivity to 440 °C (i.e., the UV exposure condition) gives a conductivity in the 10^{-3} S cm^{-1} range and this would even indicate a $p(O_2)$ of 10^{11} Pa in Fe:STO after illumination, i.e., a $\Delta\mu_{O_2}$ of 948 meV. These chemical potential changes may translate to a cell voltage when using Fe:STO as a mixed conducting electrode in an electrochemical cell with an oxygen ion conducting electrolyte, cf. similar experiments with undoped STO.[36] However, those measurements are the topic of future studies.

4. Conclusion

UV irradiation at elevated temperatures in the range of 400 °C leads to a blackening of Fe-doped $SrTiO_3$. This blackening permanently remains at room temperature and recovers only extremely slowly at about 400 °C, even at 700 °C in air it takes 720 min to recover to the initial state. Characteristic changes in UV–vis absorption spectra show that this photochromic effect is caused by a change of the Fe^{4+} concentration and thus by an oxidation of the sample. Accordingly, an increase of the oxygen content takes place in $SrTiO_3$ samples under UV, i.e., a decrease of the oxygen vacancy concentration. Impedance as well as van der Pauw measurements reveal that the (dark) hole conductivity is strongly increased after the UV exposure, in accordance with the optical studies and the suggested defect chemical changes (increase of Fe^{4+} and decrease of oxygen vacancy concentrations). The bandgap energy (2.74 eV at 440 °C) does not change by UV irradiation. The time dependence of the absorbance under UV indicates a very reasonable oxygen chemical diffusion coefficient of about 10^{-7} cm^2 s^{-1} at 440 °C, which further supports the interpretation of the observed photochromism in terms of oxygen stoichiometry changes in the entire bulk of Fe:STO. From the conductivity changes upon UV illumination we can estimate that the oxygen chemical potential in Fe:STO is enhanced by several hundred meV, corresponding to an (internal) $p(O_2)$ increase by several orders of magnitude (at least to 10^9 Pa). All together, we can conclude that the observed photochromic effect can be consistently explained by oxygen stoichiometry changes under UV and thus it is very different from the common photochromic effects in oxides caused by the activation of color centers. Rather, it is the true counterpart of the known electrocoloration of Fe:STO.

5. Experimental Section

Optical and electrochemical measurements were carried out on Fe:STO single crystals ($5 \times 5 \times 0.5$ mm^3/$10 \times 10 \times 0.5$ mm^3, (001) oriented) from Alineason Materials Technology GmbH, Germany. Laser ablation–inductively coupled plasma–mass spectrometry (LA–ICP–MS)[62,63] revealed a Fe concentration of 0.016 ± 0.002 mol% based on the Ti content (≈2.7×10^{18} Fe cm^{-3}), which is lower than the nominal value (0.16 mol%). ICP–MS measurements also showed that Fe is the predominant aliovalent cation. In a first step, all specimens were annealed for 720 min at 1000 °C in air and then cooled with 5 °C min^{-1} to eliminate potential surface defects and inhomogeneities. After the procedure we receive a smooth surface with no precipitations at the surface as sometimes reported, that we expect to be Sr-rich according to literature.[64] In ToF–SIMS measurements we observe homogeneous cation composition after the typical transient response there in the first few nanometers underneath surfaces.

For characterizing the light-induced changes, the following tools were employed. UV–vis absorption experiments were carried out on a measurement setup consisting of a heating stage, and a UV–vis system, in which a deuterium and a tungsten lamp (Edmund Optics Inc., Germany) were used as light sources and an Ocean Optics QE6500 (Halma plc, England) as spectrometer. A schematic of the setup is given in Figure 5a. The surface temperature of the Fe:STO crystal was determined on a reference sample with a sputtered thin film thermocouple. UV irradiation was performed by means of a UV–LED (365 nm, 3 W radial output) from Led Engin Inc., USA. and a quartz rod, acting as optical guide for the UV light. For in situ absorbance experiments, this quartz rod was part of the UV–vis setup (see Figure 5a), for ex situ studies, the sample was positioned in a tube furnace with the quartz rod directing light onto the sample. Additionally, various UV irradiation experiments were carried out, with parts of the sample covered by a shadow mask and oxygen diffusion profiles were calculated using the finite element method in COMSOL Multiphysics software (COMSOL AB, Sweden).

Van der Pauw experiments were used to monitor changes of the conductivity caused by a preceding illumination step (ex situ, by the UV–LED described above). Four Pt thin-film electrodes (200 nm thickness) were sputter deposited in Ar (2×10^{-2} mbar) onto the edges of $5 \times 5 \times 0.5$ mm^3 specimens using a DC magnetron sputtering system (BAL-TEC MED 020 Coating system, BalTec, Switzerland) and a shadow mask. For the actual conductivity measurements, two Keithley 2000 multimeter and a 2410 1100 V source meter (Keithley Instruments, USA) were used, with the samples being positioned in a tube furnace.

In situ observation of conductivity changes was performed by electrochemical impedance spectroscopy on a $10 \times 10 \times 0.5$ mm^3 single crystal with sputtered Pt-stripe electrodes on two edges with a distance of 5.8 mm in between (see Figure 11). The sample was positioned in a tube furnace with UV–LED light exposure by means of a quartz rod at 350 and 400 °C. UV illumination and oxygen incorporation took place at the free Fe:STO surface and caused a conductivity increase and a coloration of the single crystal. The sample's impedance was measured before, during, and after UV exposure by means of a Novocontrol Alpha-A high-performance frequency analyzer with an Electrochemical Test Station POT/GAL 30 V/2 A or a Novocontrol Alpha-A high-performance frequency analyzer, respectively (both Novocontrol Technologies GmbH & Co. KG, Germany).

Acknowledgements

The authors like to acknowledge the financial support and open access funding provided by Austrian Science Fund (FWF) (project: F4509-N16, FOXSI) and funding from the European Union's Horizon 2020 research and innovation programme under grant agreement No. 824072. Andreas Limbeck and Stefan Smetaczek are gratefully thanked for ICP–MS measurements. Tobias Huber and Huber Scientific are gratefully thanked for building many of the measurement setups.

Conflict of Interest

The authors declare no conflict of interest.

Keywords

defect chemistry, oxygen vacancies, photocoloration, $SrTiO_3$

Received: January 8, 2019
Revised: March 12, 2019
Published online:

[1] R. Merkle, J. Maier, *Angew. Chem., Int. Ed.* **2008**, *47*, 3874.
[2] M. Wojtyniak, K. Szot, R. Wrzalik, C. Rodenbücher, G. Roth, R. Waser, *J. Appl. Phys.* **2013**, *113*, 083713.
[3] U. Aschauer, N. A. Spaldin, *J. Phys.: Condens. Matter* **2014**, *26*, 122203.
[4] R. Astala, P. D. Bristowe, *J. Phys.: Condens. Matter* **2002**, *14*, 13635.
[5] H. Shen, Y. Song, H. Gu, P. Wang, Y. Xi, *Mater. Lett.* **2002**, *56*, 802.
[6] J. W. Fergus, *Sens. Actuators, B* **2007**, *123*, 1169.
[7] W. Menesklou, H.-J. Schreiner, K. H. Härdtl, E. Ivers-Tiffee, *Sens. Actuators, B* **1999**, *59*, 184.
[8] D. M. Hill, H. M. Meyer, J. H. Weaver, *J. Appl. Phys.* **1989**, *65*, 4943.
[9] R. Waser, R. Dittmann, G. Staikov, K. Kristof, *Adv. Mater.* **2009**, *21*, 2632.
[10] W. Jung, H. L. Tuller, *Adv. Energy Mater.* **2011**, *1*, 1184.
[11] D. C. Johnson, A. L. Prieto, *J. Power Sources* **2011**, *196*, 7736.
[12] A. Rothschild, W. Menesklou, H. L. Tuller, E. Ivers-Tiffee, *Chem. Mater.* **2006**, *18*, 3651.
[13] R. Moos, K. H. Härdtl, *J. Am. Ceram. Soc.* **1997**, *80*, 2549.
[14] I. Denk, W. Münch, J. Maier, *J. Am. Ceram. Soc.* **1995**, *78*, 3265.
[15] J. N. Baker, P. C. Bowes, D. M. Long, A. Moballegh, J. S. Harris, E. C. Dickey, D. L. Irving, *Appl. Phys. Lett.* **2017**, *110*, 122903.
[16] J.-J. Wang, H.-B. Huang, T. J. M. Bayer, A. Moballegh, Y. Cao, A. Klein, E. C. Dickey, D. L. Irving, C. A. Randall, L.-Q. Chen, *Acta Mater.* **2016**, *108*, 229.
[17] J. Kubacki, D. Kajewski, J. Goraus, K. Szot, A. Koehl, C. Lenser, R. Dittmann, J. Szade, *J. Chem. Phys.* **2018**, *148*, 154702.
[18] F. J. Morin, J. R. Oliver, *Phys. Rev. B* **1973**, *8*, 5847.
[19] R. Waser, T. Bieger, J. Maier, *Solid State Commun.* **1990**, *76*, 1077.
[20] R. Merkle, R. A. De Souza, J. Maier, *Angew. Chem., Int. Ed.* **2001**, *40*, 2126.
[21] B. W. Faughnan, *Phys. Rev. B* **1971**, *4*, 3623.
[22] K. W. Blazey, O. F. Schirmer, W. Berlinger, K. A. Müller, *Solid State Commun.* **1975**, *16*, 589.
[23] D. N. Mueller, M. L. Machala, H. Bluhm, W. C. Chueh, *Nat. Commun.* **2015**, *6*, 6097.
[24] D. N. Mueller, R. A. DeSouza, J. Brendt, D. Samuelis, M. Martin, *J. Mater. Chem.* **2009**, *19*, 1960.
[25] T. Bieger, J. Maier, R. Waser, *Sens. Actuators, B* **1992**, *7*, 763.
[26] T. Bieger, H. Yugami, N. Nicoloso, J. Maier, R. Waser, *Solid State Ionics.* **1994**, *72*, 41.
[27] S. Rodewald, J. Fleig, J. Maier, *J. Am. Ceram. Soc.* **2000**, *83*, 1969.
[28] J. Blanc, D. L. Staebler, *Phys. Rev. B* **1971**, *4*, 3548.
[29] R. Waser, T. Baiatu, K.-H. Härdtl, *J. Am. Ceram. Soc.* **1990**, *73*, 1645.
[30] M. Kubicek, R. Schmitt, F. Messerschmitt, J. L. M. Rupp, *ACS Nano* **2015**, *9*, 10737.
[31] T.-F. Zhang, X.-G. Tang, Q.-X. Liu, Y.-P. Jiang, *J. Alloys Compd.* **2018**, *730*, 516.
[32] R. Waser, M. Aono, *Nat. Mater.* **2007**, *6*, 833.
[33] R. Waser, *J. Am. Ceram. Soc.* **1990**, *73*, 1654.
[34] J. Janek, C. Korte, *Solid State Ionics.* **1999**, *116*, 181.
[35] R. E. W. Casselton, *J. Appl. Electrochem.* **1974**, *4*, 25.
[36] G. Walch, B. Rotter, G. C. Brunauer, E. Esmaeili, A. K. Opitz, M. Kubicek, J. Summhammer, K. Ponweiser, J. Fleig, *J. Mater. Chem. A* **2017**, *5*, 1637.
[37] F. V. E. Hensling, D. J. Keeble, J. Zhu, S. Brose, C. Xu, F. Gunkel, S. Danylyuk, S. S. Nonnenmann, W. Egger, R. Dittmann, *Sci. Rep.* **2018**, *8*, 8846.
[38] M. Akiyama, *Appl. Phys. Lett.* **2010**, *97*, 181905.
[39] S. Kamimura, H. Yamada, C.-N. Xu, *Appl. Phys. Lett.* **2013**, *102*, 031110.
[40] Y. J. Bai, W. Z. Liu, A. Chen, L. Shi, X. H. Liu, Z. Zi, *Appl. Phys. Lett.* **2018**, *112*, 211101.
[41] Y. Jin, Y. Hun, Y. Fu, Z. Mu, G. Ju, *Mater. Lett.* **2014**, *134*, 187.
[42] S. Bogati, R. Basnet, W. Graf, A. Georg, *Sol. Energy Mater. Sol. Cells* **2017**, *166*, 204.
[43] M.-H. Huang, J.-Y. Xia, Y.-M. Xi, C.-X. Ding, *J. Eur. Ceram. Soc.* **1997**, *17*, 1761.
[44] M. Akiyama, H. Yamada, K. Sakai, *J. Ceram. Soc. Jpn.* **2011**, *119*, 338.
[45] D. M. Tobaldi, M. J. Hortiguela Gallo, G. Otero-Irurueta, M. K. Singh, R. C. Pullar, M. P. Seabra, J. A. Labrincha, *Langmuir* **2017**, *33*, 4890.
[46] D. Cibrev, M. Jankulovska, T. Lana-Villarreal, R. Gomez, *ACS Appl. Mater. Interfaces* **2014**, *6*, 10304.
[47] V. N. Kuznetsov, N. I. Glazkova, R. V. Mikhaylov, N. Serpone, *Photochem. Photobiol. Sci.* **2016**, *15*, 1289.
[48] J. Fleig, M. Kubicek, *Nat. Mater.* **2018**, *17*, 389.
[49] K. Szot, W. Speier, R. Carius, U. Zastrow, W. Beyer, *Phys. Rev. Lett.* **2002**, *88*, 075508.
[50] K. K. Adepalli, J. Yang, J. Maier, H. L. Tuller, B. Yildiz, *Adv. Funct. Mater.* **2017**, *27*, 1700243.
[51] D. Marrocchelli, L. Sun, B. Yildiz, *J. Am. Chem. Soc.* **2015**, *137*, 4735.
[52] E. M. Rockkar, R. A. Forman, *Phys. Status Solidi A* **1976**, *33*, K91.
[53] K. W. Blazey, *Phys. Status Solidi A* **1976**, *38*, K97.
[54] J. Maier, *Physical Chemistry of Ionic Materials Ions and Electrons in Solids*, Wiley, Chichester, UK **2004**.
[55] T. Bieger, J. Maier, R. Waser, *Solid State Ionics.* **1992**, *53–56*, 578.
[56] K. van Benthem, C. Elsässer, R. H. French, *J. Appl. Phys.* **2001**, *90*, 6156.
[57] S. Kiran, S. Naveen Kumar, K. C. Yogananda, D. Rangappa, *J. Mater. Sci.: Mater. Electron.* **2018**, *29*, 12681.
[58] S. K. O'Learyur, P. K. Lim, *Solid State Commun.* **1997**, *104*, 17.
[59] P. S. Shinde, G. H. Go, W. J. Lee, *J. Mater. Chem.* **2012**, *22*, 10469.
[60] L. J. van der Pauw, *Philips Res. Rep.* **1958**, *13*, 1.
[61] L. J. van der Pauw, *Philips Tech. Rev.* **1958/1959**, *20*, 220.
[62] G. Bauer, A. Limbeck, *Spectrochim. Acta, Part B* **2015**, *113*, 63.
[63] F. A. Orellana, C. G. Gálvez, F. A. Orellana, C. G. Gálvez, M. T. Roldán, C. García-Ruiz, M. T. Roldán, C. García-Ruiz, *TrAC. Trends Anal. Chem.* **2013**, *42*, 1.
[64] K. Szot, W. Speier, U. Breuer, R. Meyer, J. Szade, R. Waser, *Surf. Sci.* **2000**, *460*, 112.